

Article

Assessment of the Impacts of Climate Change on the Water Quality of a Small Deep Reservoir in a Humid-Subtropical Climatic Region

Chih-Hua Chang ^{1,*}, Long-Yan Cai ^{1,*}, Tsair-Fuh Lin ¹, Chia-Ling Chung ¹,
Leon van der Linden ² and Michael Burch ²

¹ Department of Environmental Engineering and Global Water Quality Research Center, National Cheng Kung University, Tainan 70101, Taiwan; E-Mails: tflin@mail.ncku.edu.tw (T.-F.L.); chung@cycu.org.tw (C.-L.C.)

² Australian Water Quality Centre (AWQC), SA Water, Adelaide, SA 5001, Australia; E-Mails: leon.vanderlinden@sawater.com.au (L.L.); mike.burch@sawater.com.au (M.B.)

* Authors to whom correspondence should be addressed; E-Mails: chihhua@mail.ncku.edu.tw (C.-H.C.); cly@xmu.edu.cn (L.-Y.C.); Tel.: +886-6-275-7575 (ext. 65826) (C.-H.C.); +886-6-275-7575 (ext. 65850#47) (L.-Y.C.); Fax: +886-6-275-2790 (C.-H.C.); +886-6-275-2790 (L.-Y.C.).

Academic Editor: Jun Xu

Received: 5 February 2015 / Accepted: 10 April 2015 / Published: 20 April 2015

Abstract: Surface water quality has been identified as potentially vulnerable to climate change. This study assesses the impacts of climate change on the water quality of Hsinshan Reservoir, Taiwan, through CE-QUAL-W2 simulations. The model parameters were calibrated by field data collected during 2004–2008, and verified against observations made during 2009–2012. The projected temperature and precipitation data for the near- and long-term future were downscaled to regional and daily scales, and used to simulate the projected changes in water quality through the validated model. The simulation results were reported as probability-based cumulative distribution functions to assess the impacts of climate change on water quality. The results indicated that the intensified thermal stratification caused by the rising temperature is the primary driver of water quality decline, which increases the probability of deep-layer oxygen depletion and the flux of limiting nutrients for algae growth, resulting in a higher risk of algal blooms and eutrophication. The adaptation strategies of multilevel-intake operations and increasing bottom-layer dissolved oxygen without destratification are recommended.

Keywords: reservoir; climate change; water quality; risk; CE-QUAL-W2

1. Introduction

The warming of the global climate system is now unequivocal and will continue to grow due to increased anthropogenic greenhouse gas emissions [1], which can induce a variety of changes in freshwater resources [2]. Changes in the temperature and radiation balance under a warmer climate are consistently associated with changes in essential components of the hydrological cycle and hydrological systems, e.g., changing precipitation patterns (extreme) and increasing atmospheric water vapor and evaporation [1,3,4]. As a result, large-scale artificial water storage facilities, such as dam reservoirs, are predicted to play a more important role as a buffer against rainfall variability in support of economic development [5]. In addition, a warmer climate is generally projected to have adverse impacts on water quality and intensify many forms of water pollution [6–8]. Therefore, to ensure the safety and security of storage water, it is important to assess the impacts of climate change on water quality.

Despite the fact that a number of studies have evaluated the impacts of climate change on the water quality of freshwater ecosystems [9–12], e.g., natural lakes and streams, limited information is available for man-made ecosystems, such as reservoirs. Reservoirs represent hybrid systems of rivers and lakes [6], and their water quality is not only influenced by human activities, but also by natural factors, such as climate change. Closed water basins, like lakes and reservoirs, are especially sensitive to climate change [13], and many studies indicate that increases in water temperature are consistently associated with the increased thermal stratification of such water bodies. For example, it has been shown that the warmer climate intensifies the thermal stratification and stability of Lake Tahoe in the USA [12]. Similarly, the duration of thermal stratification is projected to be prolonged in the Grafham Reservoir in the UK [14], due to the increased air temperature. Under these conditions, the periods of overturn that bring a fresh supply of oxygen to the deeper layers would also be prolonged, resulting in an increased level of nutrients after thermal stratification [15]. Regional studies in Lake Ringsjön (Sweden) and in Lake Okareka (New Zealand) both indicate that the projected increases in air temperature and precipitation are very likely to increase the level of total phosphorus (TP), total nitrogen (TN) and chlorophyll-*a* (Chl-*a*) [16,17]. However, similar climate change patterns may not always lead to consistent changes in lake water quality parameters. For example, increases in air temperature and precipitation since the 1980s have not caused any obvious changes in TP and Chl-*a* in Loch Leven in the UK [18]. Furthermore, in a climate zone that is warmer but has decreased precipitation, TN was observed to increase, while TP and Chl-*a* declined, in an experimental lakes area in Northwestern Ontario [19]. The varied conclusions of these works are related to site-specific conditions and different patterns of climate change. Moreover, the sensitivities of reservoirs of different ages to climate change can vary markedly when a reservoir changes from an abiotic to a biotic ecosystem, like a lake [13]. Therefore, empirical studies which assess the impacts on reservoirs on a regional or climate-specific scale are needed to help determine the appropriate adaptation strategies for the water industry [20].

The temperate zones in Asia are generally experiencing more severe temperature increases than other temperate zones around the world [21]. The main island of Taiwan is located in the Western Pacific and is crossed by the Tropic of Cancer, where the rate of increase in the near-ground average air temperature has been shown to be twice the global average (0.6–0.7 °C) [22], and the precipitation intensity, seasonal variability, and extremes have generally increased over the past 50 years [23]. Because of the significant variations in seasonal precipitation, Taiwan is a region that is water-stressed, although the country has a high density of about 60 artificial reservoirs with a total area of around 360,000 km² that are used for various purposes. Hsinshan Reservoir (HSR) is a small, deep, off-channel drinking water reservoir located in Northern Taiwan. As the area is highly vulnerable to climate change [24], this type of reservoir deserves particular attention, and is the focus of the current work.

One effective way to evaluate the effects of climate change on ecosystems and water quality is to use numerical models. Several simulation models have been widely used to study freshwater ecosystems [16,17,25–27], such as the integration of one-dimensional Dynamic Reservoir Simulation Model and Computational Aquatic Ecosystem Dynamics Model (DYRESM-CAEDYM), the applications of two-dimensional water quality and hydrodynamic model supported by the U.S. Army Corps of Engineers (CE-QUAL-W2), and the three-dimensional Hydrodynamic Model Water Modeling System (MOHID) developed by Technical University of Lisbon, Portugal. The projected changes in future climate, especially those on a regional scale, are the most important information that is needed to predict the effects of climate change on reservoir water quality. However, changes in climate on in the local scale are generally difficult to reliably predict. Therefore, most related studies use climate data, which was downscaled to the scale of interest from the outputs of Atmosphere–Ocean Global Circulation Models (AOGCMs). Although a considerable amount of research on the impacts of climate change on reservoirs has been undertaken, due to significant uncertainties with regard to the climate data [28,29] and the inconsistent modeling approaches applied, these impacts on water quality are still poorly understood [1]. In addition, there is a need to develop methods to adapt the projected climate change data to a scale and format that is both meaningful and compatible with impact assessment models [30].

This study focused on HSR and used the CE-QUAL-W2 model to study the impacts of climate change on risks to water quality under A1B and A2 scenarios for the near- (2020–2039) and long-term future (2080–2099). Compared with other reservoir/climate studies, the research in this work focuses on three particular aspects. First, we assess the impacts of climate change on the water quality for an artificial dam reservoir, which differs from natural lakes in geometric shape and the method of water recharge. Second, this work performs in a vulnerable region where the site- and climate-specific information is limited and hence needed. Third, the climate-reservoir modeling results utilize probability-based cumulative distribution functions, which are different from common statistical approaches, such as averages and correlations [14,31]. Specifically, the intent was to (1) calibrate and validate the CE-QUAL-W2 model; (2) investigate the risks to water quality under A1B and A2 scenarios for the near- and long-term future; and (3) put forward risk-based adaptation and planning strategies for improving water quality and ensuring the safety of drinking water.

2. Materials and Methods

2.1. Study Area

The Hsinshan Reservoir (121°42'08"–121°42'42" E, 25°07'23"–25°08'04" N) is located on a branch of Keelung River in the northern part of Taiwan (Figure 1). As one of the major drinking water reservoirs in Northern Taiwan, HSR serves a population of more than 400,000 residents in Keelung City and New Taipei City. The reservoir was constructed in 1980, with a maximum capacity of $9.7 \times 10^6 \text{ m}^3$ at 86 m above sea surface level.

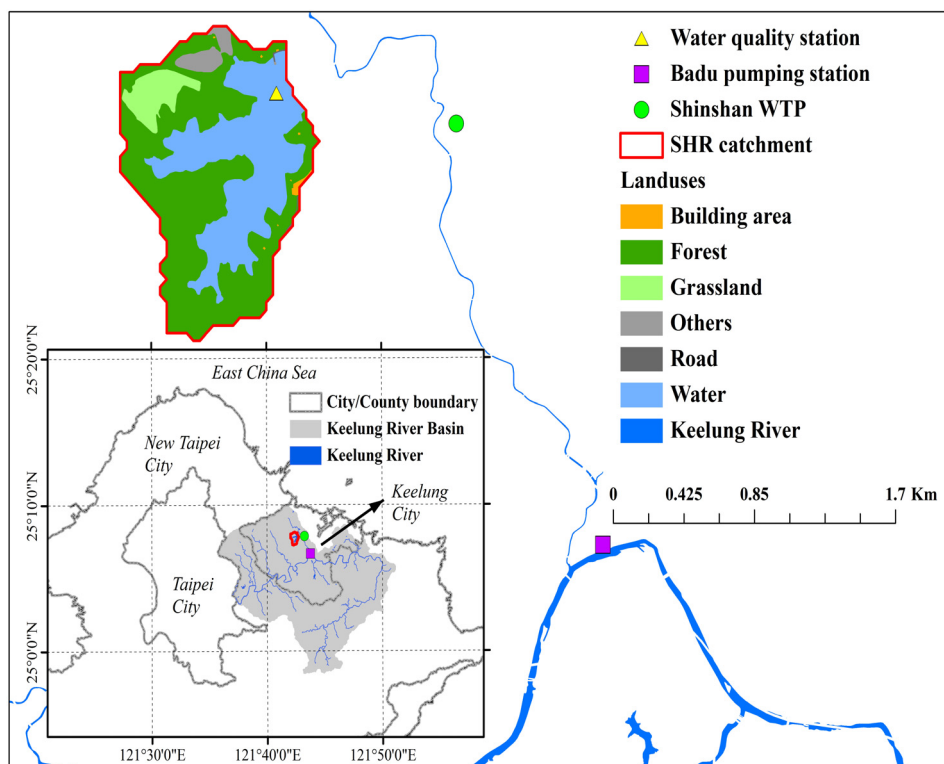


Figure 1. The geographic location of Hsinshan reservoir.

As shown on Figure 1, the water pumped from Keelung River through Badu Pumping Station was designed for Hsinshan water treatment plant (WTP) as the primary source of raw water. The catchment of Badu Pumping Station is a designated Drinking Water Source Protection Area, where natural forest land are mostly conserved and high pollution activities in this area are prohibited. Sources of pollution affecting the quality of the pumped water entering HSR include untreated municipal wastewater, polluted runoff from urban area, and natural nonpoint source pollution. Because the pumped water is less stable in quantity and quality than that from a reservoir, the WTP takes water stored in HSR as an alternative when the primary source (Keelung River) is not sufficient to meet demand with regard to quantity (mostly in the dry season) and quality (in both the dry and wet seasons). Therefore, water in the reservoir is recharged occasionally by diverting additional/bypassed “raw water” from the WTP to HSR. As a result of multi-source operation in the WTP, HSR is an indirect, off-channel reservoir of Keelung River in which 35% of the storage water is contributed by the 1.6 km² natural catchment ($4.5 \times 10^6 \text{ m}^3/\text{year}$) through direct precipitation and runoff (hereafter referred as “direct water”), and

another 65% (7.0×10^6 m³/year) comes from the recharged water from Hsinshan WTP (hereafter referred as “recharged water”). Note that there is no standard operation procedure indicating the timing, quality or amount of recharge.

The climate is warm and humid in Taiwan because of the surrounding low-latitudes within the Pacific Ocean. The average daily maximum air temperature in HSR ranges from 18 °C in January to 33 °C in July. HSR receives abundant rainfall throughout the year, with an average annual precipitation of over 3700 mm. There are no distinct dry and wet seasons, but higher precipitation is expected during the fall monsoon season (September to November) and winter months (December to February).

HSR has a temperature profile typical for subtropical lakes, which ranges from 16 to 32 °C at the surface layer, and 14 to 24 °C at the bottom layer. Generally, there is only one annual thermal stratification period, which starts in late spring and ends in early fall for HSR. The water column is well mixed and is in contact with oxygen from the atmosphere from fall to spring. The levels of nutrients at the hypolimnion layer were significantly higher during the stratification period [32]. The seasonal Carlson Trophic State Index (CTSI) obtained from 2004–2012 indicated that HSR is between a mesotrophic state and a eutrophic state. Seasonal CTSI and the frequency of algal bloom events are higher during the springtime (April to June) [32].

2.2. CE-QUAL-W2 Model

The CE-QUAL-W2 (W2) is a two-dimensional, hydrodynamic, and water quality simulation model [33], which was developed by the Environmental and Hydraulics Laboratory of the US Army Engineer Water-ways Experiment Station. The W2 model uses finite-difference method to approximate the solution for laterally averaged equations of fluid motion. The model has the capabilities of simulating free surface elevation, pressure, density, vertical and horizontal velocities, and constituent concentration and transport [34]. W2 has been under continuous development since 1975 [33], and was particularly popular in simulating basic eutrophication processes in stratified water systems [25,26,33,35,36], such as the relationships between temperature, dissolved oxygen and algae in a natural lake [26]; and the association between organic matter and sediment in a man-made reservoir [35]. In recent years, this model has been used to evaluate the impacts of climate change on reservoir water quality to make adaptation and planning decisions for optimized water treatment plant operations [14,24]. The W2 model version 3.6 released in 2012 was used in this work, which is currently maintained and continually updated by the Water Quality Research Group (WQRG) at Portland State University [33], USA. Because the model assumes lateral homogeneity, it is most suited to narrow and deep-water bodies where lateral variations in both hydrodynamic and water quality variables are minimal [33,34]. In this study, the long, deep and narrow shape of the HSR reservoir justifies the choice of the W2 model to predict the hydrodynamic and water quality variables.

According to the physical layout of HSR (Figure 1), there are no significant tributaries in the catchment; it is assumed that one computational branch grid is sufficient to represent the entire waterbody. The horizontal and vertical spacing of 100–10,000 m and 0.2–5 m was suggested, respectively, by Cole and Scott [33] to define the geometry of the single branch grid in W2 for capturing the water quality gradients efficiently and maintaining the numerical stability. Based on these recommended range of branch grid dimensions and a topographic map, we divided the main

branch into 11 longitudinal segments (two for boundary conditions, zero length) having the length of 80–220 m, and 25 to 38 one-meter thick vertical layers. Note that the nine divided segments were identified from the topographic map. Initially it was assumed that each segment layer (cell) has a relatively constant width. The best-fitting width for each cell was then determined through multiple iterations with the help of a volume-area-elevation table provided by the Taiwan Water Corporation (TWC). As the result, the x - z computational grids representing the waterbody of HSR are shown in Figure 2. The water quality sampling station (Station 1) and the water inlet/outlet of HSR are located in segments 1 and 3, respectively.

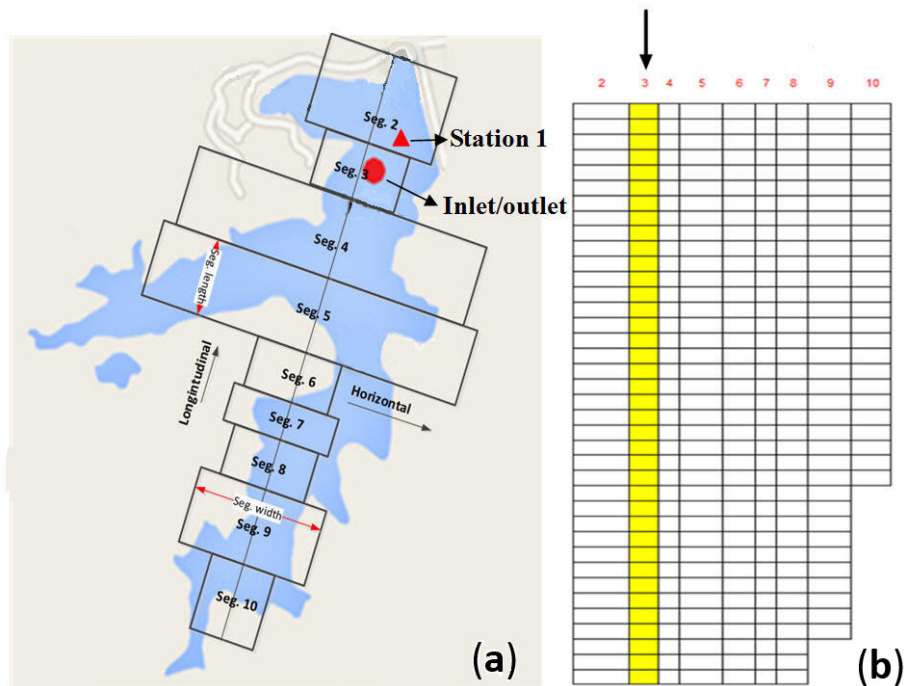


Figure 2. Model segmentations of HSR. (a) Longitudinal segments; (b) Vertical layers.

The quantity and quality of direct flows were estimated by the amount of precipitation and rainwater quality observed in the Keelung City, and the event mean concentrations of runoff from different land use areas in Taiwan [37,38]. Note that the catchment runoff was obtained from the water balance of observed water level, recharged flow, evaporation, outflow and precipitation. The volumetric mass loading of recharged flow was calculated by using the recharged flow rate, and Keelung River's water quality was measured at the Hsinshan WTP and the Badu pumping station. The validated model was then employed to evaluate the impacts of climate change (*i.e.*, changes in temperature and direct precipitation) on the direct inflow quantity and reservoir water quality in the near- and long-term future scenarios. It is assumed that the quality of catchment runoff, rainwater and recharged water, as well as the patterns of water recharge and outflow, remain unchanged in the future and hence these are set to the same conditions as those of 2004–2012.

2.3. Climate Change Data

The climate change dataset used in this study was provided by Taiwan Climate Change Projection and Information Platform Project (TCCIP) [39], which consists of 24 spatially downscaled AOGCM

outputs of projected changes in precipitation and temperature for the near- (2020–2039) and long-term (2080–2099) under different greenhouse gas emission scenarios. Note that the 24 AOGCMs selected by TCCIP were the same set of models described in the Fourth Assessment Report of Intergovernmental Panel on Climate Change (IPCC AR4). The downscaled outputs of AOGCMs can be seen as the outputs from 24 regional climate models (RCMs), with a resolution of $0.25^\circ \times 0.25^\circ$ and $0.5^\circ \times 0.5^\circ$ for precipitation and temperature, respectively.

In order to run the W2 model for HSR on a daily basis, an additional downscaling step from RCM was performed in this study using a pattern scaling method [40]. This is performed by mapping the cumulative distribution function (CDF) of daily climate observations (2004–2012, Keelung Weather Station) to that interpolated from the ensemble of 24 RCM outputs using an empirical CDF. Three kinds of statistical techniques are commonly employed to condition the RCM output [41]: quantile-quantile mapping (QM), distribution-based scaling (DBS) and simple direct method. Although data conditioned by DBS has been shown to perform better than other methods for precipitation from RCMs [41], it is also suggested that QM can improve systematic biases throughout the probability distribution of climate differences, and hence improves the adjustments of extremes. Studies for the assessment of the impacts of climate change on water resources in South Australia indicate that the QM method is appropriate for daily climate data production, due to its higher forecast accuracy compared to other model-output-statistics analysis approaches [40,42]. In order to condition for extremes in the output of RCM data in this study, the QM method was utilized. The CDF patterns learned from the QM procedure were then applied to extrapolate the 24 RCM outputs of future climate data on a daily basis.

In addition, the A1B and A2 emission scenarios were chosen as they were the most commonly used scenarios for planning climate adaptation strategies in Taiwan [43]. The A1B scenario assumes a balanced mix of technologies and supply sources, with technology improvements and resource assumptions such that no single source of energy is overly dominant. The A2 scenario assumes relatively slow demographic transition and slow convergence in regional fertility patterns, with slow end-use and supply-side energy efficiency improvements, such that there is delayed development of renewable energy and no barriers to the use of nuclear energy [44].

With 24 AOGCM outputs, two emission scenarios and two time projected periods evaluated in this study, there are a total of 96 sets of future climate data that will be produced for the assessment of the impacts of climate change on water quality using the W2 model. Because of the similarity in trends and distribution patterns between climate outputs from 24 AOGCMs, it is impractical to run each of the 96 sets of climate data. First, the averaged value of 24 AOGCM outputs was selected to represent the multi-model ensemble forecast. Second, we analyzed the CDFs of 24 AOGCM outputs under each scenario and period, and selected the models located at the lower limit of 10% (LL 10%), lower limit of 25% (LL 25%), upper limit of 75% (UL 75%), and upper limit of 90% (UL 90%) tiles to efficiently cover the range of multi-model outputs. The selected climate models for each percentage tile are listed in Table 1.

Table 1. Selected AOGCM climate outputs for the simulation of the impacts of climate change on water quality.

Climate Variable	Selected Climate Model			
	2020–2039		2080–2099	
	A1B	A2	A1B	A2
Temperature LL 10%	MRI-CGCM 2.3.2	CGCM 3.1 (T47)	AOM 4x3	ECHAM 4.6
Temperature LL 25%	AOM 4 × 3	ECHAM 5/MPI-OM	AOM 4x3	PCM 1.0
Temperature UL 75%	CCSM 3.0	CCSM 3.0	MIROC 3.2	MIROC 3.2
Temperature UL 90%	MIROC 3.2	CCSM 3.0	MIROC 3.2	MIROC 3.2
Rainfall LL 10%	BCM 2.0	BCM 2.0	BCM 2.0	BCM 2.0
Rainfall LL 25%	BCM 2.0	BCM 2.0	GISS Model ER	GISS Model ER
Rainfall UL 75%	BCM 2.0	BCM 2.0	CM 2.0	BCM 2.0
Rainfall UL 90%	CSIRO Mark 3.0	CGCM 3.1 (T47)	MRI-CGCM 2.3.2	BCM 2.0

Note: AOM 4 × 3: Atmosphere–Ocean Model (4° longitude by 3° latitude resolution), NASA, USA; BCM: Bergen Climate Model, University of Bergen, Norway; CCSM: Community Climate System Model, NCAR, USA; CGCM (T47): Coupled Global Model (T47: spatial resolution is roughly 3.75° latitude/longitude and 31 levels in the vertical), Canadian Centre for Climate Modelling and Analysis; CSIRO: Commonwealth Scientific and Industrial Research Organization, Australia; ECHAM5/MPI-OM: Coupling of atmospheric general circulation model version 5 and the Max Planck Institute ocean model, Germany; GISS Model ER: the Goddard Institute for Space Studies (GISS) ModelE atmospheric code and Russell ocean model, USA; MIROC: Model for Interdisciplinary Research on Climate, jointly developed in Japan by the Center for Climate System Research (CCSR), the National Institute for Environmental Studies (NIES), the Frontier Research Center for Global Change (FRCGC), and the Japan Agency for Marine–Earth Science and Technology (JAMSTEC); MRI-CGCM: Codelist for Global Circulation Models, Meteorological Research Institute, Japan; and PCM: Parallel Climate Model, NASA, USA.

2.4. Data Collection

The hydrodynamic data for model calibration and validation, which includes daily water level, storage capacity and inflow/outflow rates of HSR, were provided by TWC. The water quality data of HSR were obtained from the Environmental Water Quality Information System [45] of the Environmental Protection Administration (EPA), Taiwan. In general, water quality in drinking water reservoirs is monitored seasonally by the EPA. In addition, some daily or monthly observed surface water temperature data provided by TWC were also used in this study. The water samples were taken at approximately 9:00 a.m., at 0.5–1 m below water surface. Only water temperature, pH and dissolved oxygen (DO) were measured *in situ*; other water quality parameters were measured in the laboratory. The analytical methods used for determining water quality parameters included: (1) water temp determined by thermometer; (2) DO measured using the ion-selective-electrode method; (3) nitrate–N (NO₃–N) measured with the cadmium reduction flow injection method; (4) ammonia–N (NH₃–N) measured with the indophenol flow injection method; (5) the ortho-P (PO₄³⁻) and TP concentrations were determined by the ascorbic acid method; and (6) the chlorophyll extraction method (in 90% acetone) was applied to measure Chl-*a*. For further details on analytical methods used in this study, please refer to the Standard Methods for the Examination of Water and Wastewater issued by Taiwan Environmental Analysis Laboratory [46].

2.5. Model Calibration and Validation Procedure

The occurrence of thermal stratification can be the most important cause of water quality problems in HSR [47], which not only causes a DO deficit and nutrient-enriched hypolimnion water, but also leads to the overgrowth of blue-green algae when the water column overturns and becomes warmer during spring. First, observations of daily water level, monthly surface temperature and temperature profile were used to calibrate hydrological parameters governing the simulation of hydrodynamic variables, as well as to ensure the water budgets are consistent with grid settings. The hydrological parameters governing horizontal dispersion and bottom friction were set to default values for the Chezy friction model. Second, based on the number of water quality parameters that have been observed and are available for model calibration, six major water quality state variables associated with stratification were simulated, including DO, Chl-*a*, PO₄³⁻, NH₃-N, NO₃-N, and TP. The kinetic coefficients associated with the simulated water quality variables were calibrated within the range of values reported in the literature [33], as shown in Table 2. The default settings of the W2 model (version 3.6) were applied for the other related coefficients, which are not listed in Table 2.

Table 2. The calibrated values of W2 water quality model kinetics parameters in HSR.

Model Parameter	Parameter Range	HSR
Light extinction for pure water (m ⁻¹)	0.25 or 0.45	0.45
Light extinction due to suspended solids (m ⁻¹)	0–0.1	0.01
Suspended solids settling rate (m·d ⁻¹)	-	1.0
Sediment release rate of phosphorus (fraction of SOD)	0.001–0.015	0.023
Sediment release rate of ammonium (fraction of SOD)	0.001–0.03	0.03
Ammonia decay rate (d ⁻¹)	0.001–0.95	0.5
Nitrate decay rate (d ⁻¹)	0.03–0.15	0.03
Maximum algal growth rate (d ⁻¹)	0.17–11.0	1.3
Algal settling rate (m·d ⁻¹)	0.0–30.2	0.05
Light saturation intensity at max. photosynthetic rate (W·m ⁻²)	10–170	55
Algal half-saturation for phosphorus limited growth (g·m ⁻³)	0.001–1.52	0.0038
Algal half-saturation for nitrogen limited growth (g·m ⁻³)	0.001–4.34	0.022

Both the hydrological parameters and kinetic coefficients were calibrated by Station 1 observation data provided by the Environmental Protection Administration of Taiwan, and Taiwan Water Corporation for the period 2004–2008, and verified against to those collected for 2009–2012. These calibration and simulation results were statistically evaluated to measure for deviations between simulated and observed data, e.g., the absolute mean error (AME) and root mean square error (RMSE); and the goodness-of-fit of model, e.g., the coefficient of determination (R^2).

2.6. Risk Analysis

The simulation results for the projected water quality concentrations are organized as probability-based CDFs to identify the risks of the various impacts of climate change on water quality, *i.e.*, the probability exceeding a specific threshold value. The thresholds (low, medium, and high) represent different levels of a water quality variable that, if attained or exceeded, indicate a problem with the

water quality. For example, a threshold of 25 °C water surface temperature was used to denote the possible occurrence of algal bloom events in HSR based on historical observations [47], and 10 µg/L of Chl-*a* was used to indicate the threshold of eutrophication [48]. The risk exceedance probability is defined by:

$$\text{Risk of exceedance for } x = 1 - \text{CDF}(x) \quad (1)$$

where x is the threshold value of a water quality variable. Figure 3 shows an example of CDF curves for W2 simulated bottom-layer TP concentrations, from which the risk of TP exceeding 0.04 mg/L is 64% based on the upper 90 percentile climate model outputs.

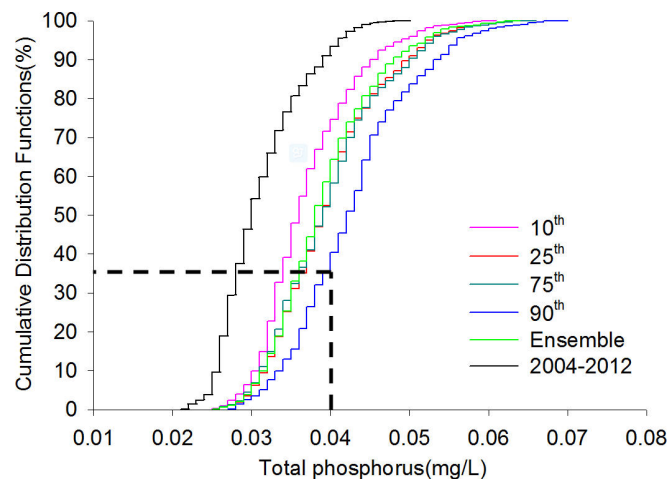


Figure 3. An example of CDF curves for bottom-layer TP concentrations simulated by W2 model and selected AOGCM climate outputs of the long-term future under A1B scenario.

3. Results and Discussion

3.1. Calibration and Validation

3.1.1. Hydrodynamic Variables

A comparison between the observed and simulated hydrodynamic variables, e.g., water level and surface temperature, at the calibration and verification periods, is shown in Figure 4. The related model performance indicators, *i.e.*, AME, RMSE and R^2 , for simulation of hydrodynamic variables are listed in Table 3. Generally, the calibrated hydrological parameters resulted in good agreement between the observations and W2 simulations. The simulation results of hydrodynamic variables in HSR using W2 model, e.g., water level and temperature, showed lower errors (RMSE and AME) and much higher R^2 values than the simulation of water quality parameters. Hydrodynamic modeling in this study was successful because of proper development of a best-fitting computational grid. The grid was developed because of the availability of both sizable amounts of HSR inflow and outflow measurements and a measured volume-area-elevation table. Hence, the accurate simulation of water levels shows that the water temperature and temperature profile can be well simulated without additional effort for model calibration.

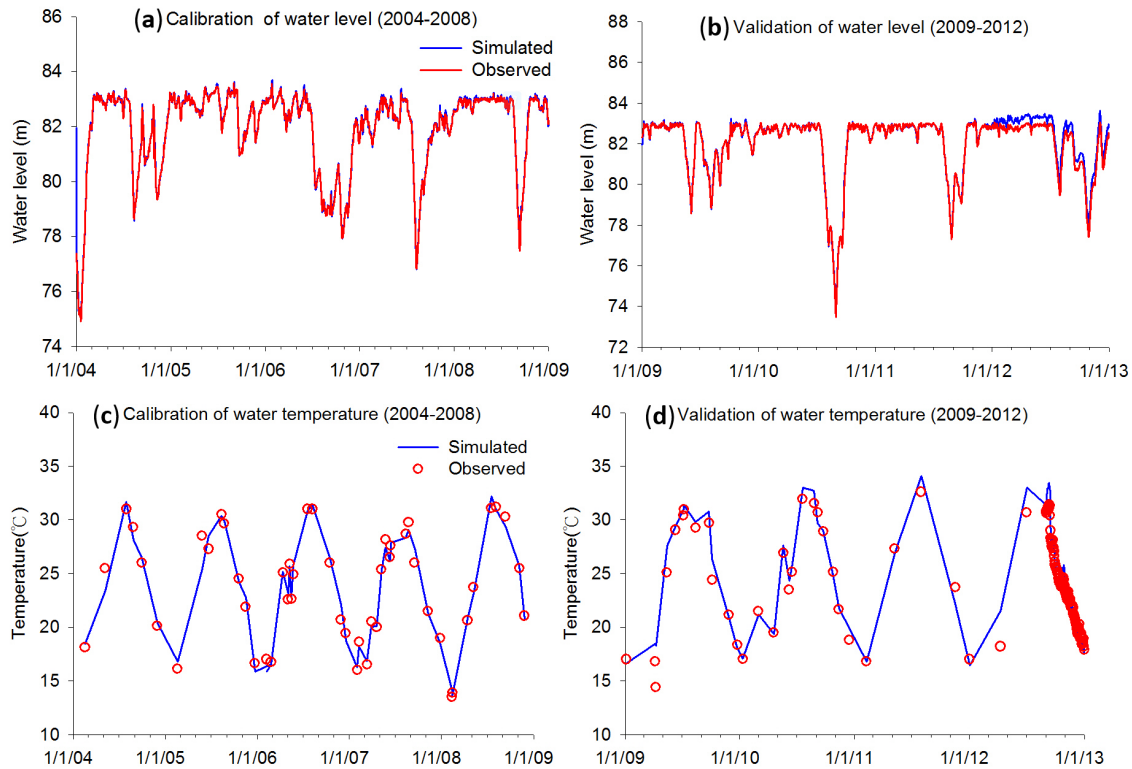


Figure 4. The calibration and validation results of W2 simulated hydrodynamic parameters at surface layer of segment 3. Sub-figures show the comparisons between W2 simulation results to: measured water level during (a) calibration and (b) validation periods; and measured water temperature during (c) calibration and (d) validation periods.

Table 3. Summary of the performance indicators for the W2 modeling of hydrodynamic and water quality variables during calibration and validation periods.

Simulated Variables	Calibration				Validation			
	<i>N</i>	<i>AME</i>	<i>RMSE</i>	<i>R</i> ²	<i>N</i>	<i>AME</i>	<i>RMSE</i>	<i>R</i> ²
Water level (m)	1827	0.14	0.20	0.98	1460	0.13	0.15	0.99
Surface temperature (°C)	50	0.59	-	0.98	154	0.68	-	0.97
DO (mg/L)	27	0.72	0.94	0.49	30	1.12	1.49	0.26
NH ₃ -N (mg/L)	22	0.019	0.025	0.51	16	0.021	0.026	0.25
NO ₃ -N (mg/L)	22	0.172	0.212	0.32	16	0.348	0.371	0.37
Ortho-P (mg/L)	22	0.009	0.011	0.38	16	0.007	0.008	0.41
TP (mg/L)	22	0.009	0.012	0.49	16	0.01	0.012	0.49
Chl- <i>a</i> (µg/L)	22	2.752	3.689	0.32	16	2.186	2.919	0.36

Notes: the number of observations (*N*); the value of absolute mean error (*AME*); the value of root mean square error (*RMSE*); and the value of determination coefficient (*R*²).

The water budget simulation shows that the water level decreased rapidly and reached its lowest level in summer due to lower precipitation and higher demand, when HSR was commonly thermal stratified. During the period of early winter to spring, the water level gradually increased and reached a relatively stable level because of abundant precipitation and recharge water from Hsinshan WTP, while the HSR is well mixed.

As shown in Figure 4c,d, the surface water temperature is governed directly by the variation of atmospheric temperature, and hence its simulation is straightforward when the given air temperature is representative of the reservoir area. Although a successful simulation of surface water temperature is not difficult, it plays an essential role in accurately deriving the thermal stratification and determining the vertical distribution of water quality variables in the reservoir.

The comparison between model-derived and observed temperature profiles shows that the thermal structure of the water column can also be well reproduced by the calibrated hydrological parameters (Figure 5). The simulated temperature profiles show that the thermal stratification in HSR developed gradually from April and became the strongest during August and September, with a 4 to 10 °C temperature difference between the surface and bottom layers. Generally, no significant thermal stratification was found with either the observations or the modeling results during October to March. Overall, the hydrodynamics simulation successfully captured the periodic process of thermal stratification and turnover in HSR.

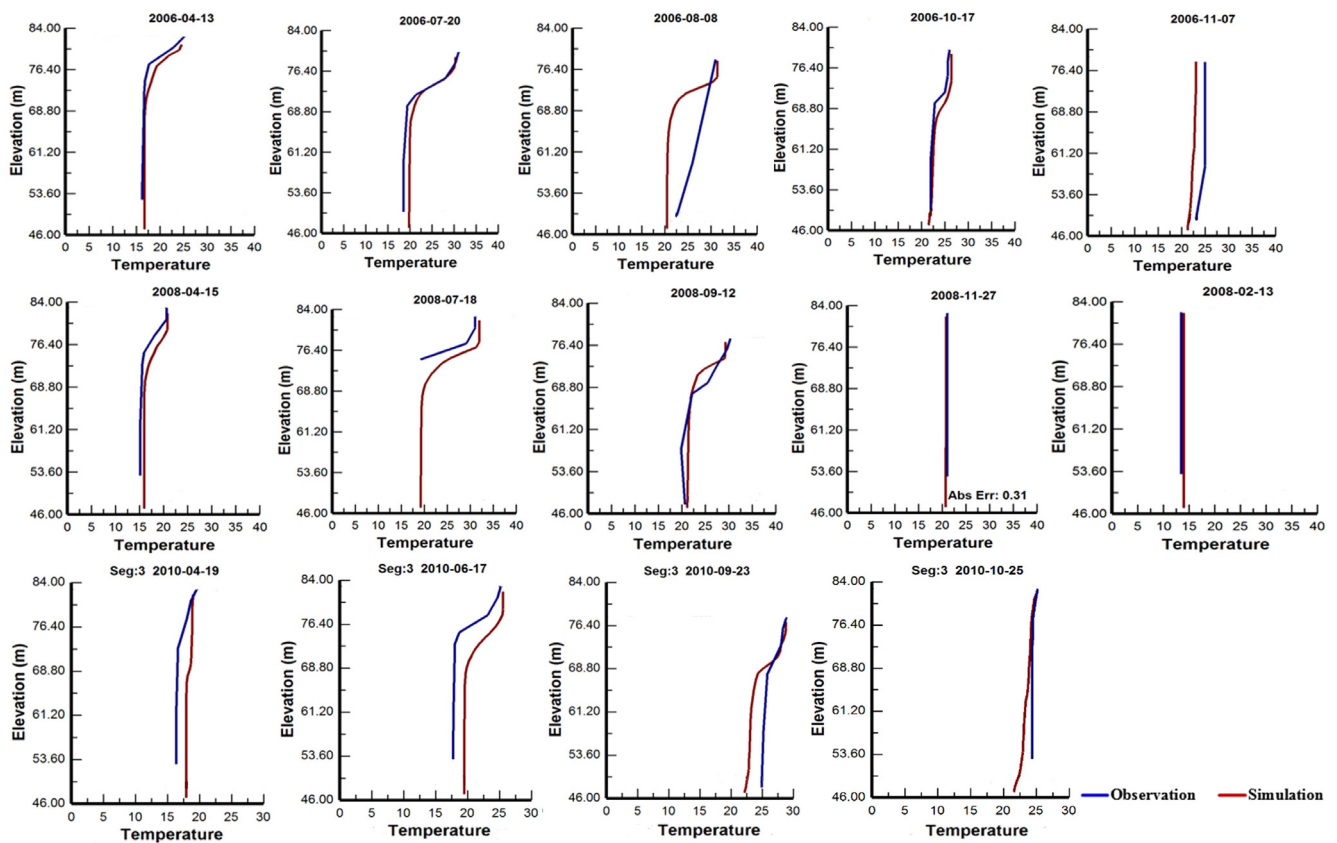


Figure 5. Comparisons between W2 simulated and observed water temperature profiles (°C) in HSR.

3.1.2. Water Quality State Variables

To assess the reliability and validity of this water quality model, multiple statistical analyses were used; these included R^2 , mean prediction errors, and Pearson’s coefficient of correlation (r). The calibration and simulation results for water quality state variables are shown in Figures 6 and 7. Clearly, the model predicted values do not match the observed data, this is reflected by higher errors

and much lower R^2 values (ranging from 0.3 to 0.5 in Table 3) than the simulation of hydrodynamic parameters. Note that the mean prediction error values for DO, $\text{NH}_3\text{-N}$, $\text{NO}_3\text{-N}$, Ortho-P, TP and Chl-*a*, are 0.42, -0.002 , -0.085 , -0.003 , 0.003, and 0.003 mg/L, respectively. Yet despite having only a moderate R^2 , the r values showed that the observed results compared to those simulated were still in fact significantly correlated ($0.5 < r < 0.7$, $p\text{-value} < 0.05$). This suggests that the simulated results can indeed capture seasonal differences relatively well. Because of this, the model used in this study should be particularly valid and useful for instances where there is great seasonal variation and hence the reservoir water quality is significantly influenced by thermal stratification.

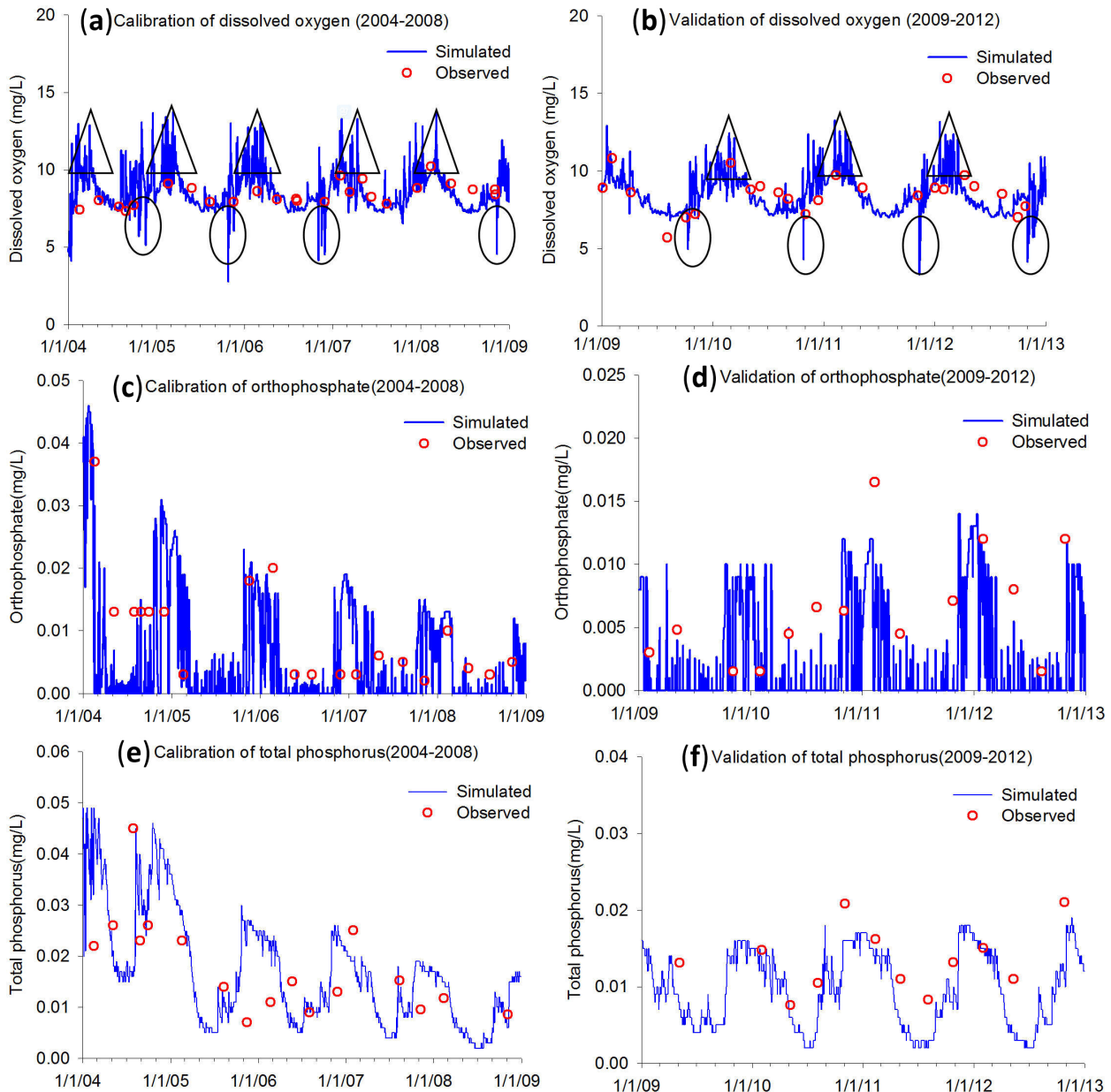


Figure 6. The calibration and validation results of W2 simulated water quality parameters at surface layer of segment 3. Sub-figures show the comparisons between W2 simulation results to: observed DO concentrations during (a) calibration and (b) validation periods; observed ortho-P concentrations during (c) calibration and (d) validation periods; and observed TP concentrations during (e) calibration and (f) validation periods.

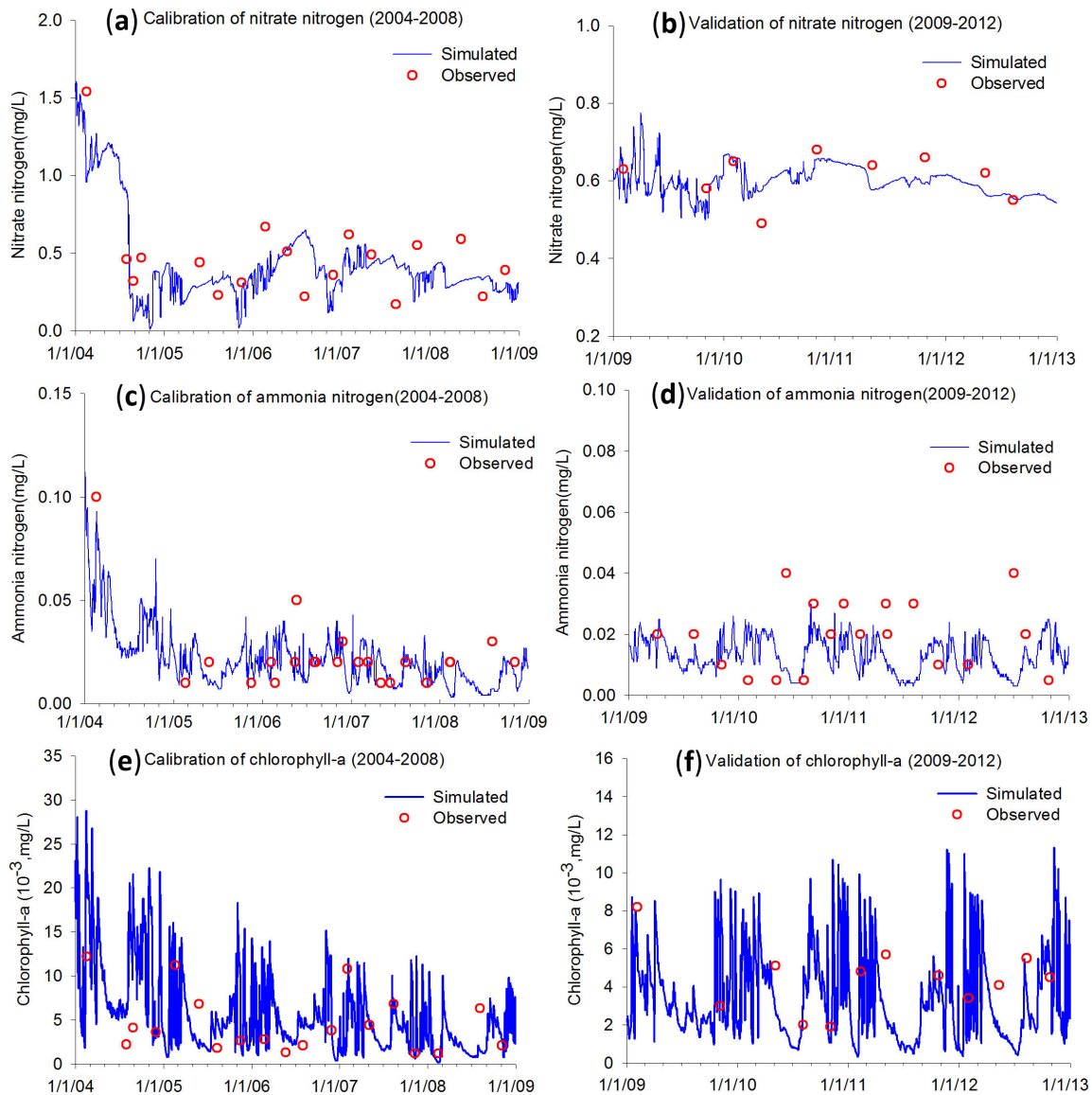


Figure 7. The calibration and validation results of W2 simulated water quality parameters at surface layer of segment 3. Sub-figures show the comparisons between W2 simulation results to: observed $\text{NO}_3\text{-N}$ concentrations during (a) calibration and (b) validation periods; observed $\text{NH}_3\text{-N}$ concentrations during (c) calibration and (d) validation periods; and observed Chl-*a* concentrations during (e) calibration and (f) validation periods.

Dissolved oxygen is the most important water quality variable determining the health status of an aquatic ecosystem [49]. In HSR, the DO concentrations in the surface layer were commonly at a saturation level, and this can then become supersaturated (triangles marked in Figure 6a,b and undergo higher day and night fluctuations during March and April, because of elevated photosynthetic activity of algae. The phenomenon of DO supersaturation was insignificant during summer, when the reservoir was experiencing thermal stratification. Significant fluctuations in surface DO were again simulated during October to November, due to two simultaneous processes occurring: (1) low-DO from the hypolimnion was upwelling towards the reservoir surface; (2) cooler weather tended to raise the solubility of DO. Consequently, the surface DO was generally increasing during this “turnover” period, but some “oxygen deficit” points were found in the simulation results (circles marked in Figure 6a,b).

Low-DO at the hypolimnion would significantly accelerate the release of phosphorus from sediment, and thus promote the growth of algae through “turnover” (October to May) [50]. Evidence for this “turnover” or the upwelling of nutrient-rich water originating from the hypolimnion is also shown in the time series plots of ortho-P and TP (Figure 6c–f)). It is speculated that phosphorus is one of indicative factors causing eutrophication [51]. However, the increased ortho-P and TP did not immediately trigger a significant growth of algae, because of the lower water temperatures from October to December. As shown in Figures 7e,f the overgrowth of algae was significant during February to May following the winter overturn, due to the combination of nutrient-rich water and warmer weather. Therefore, “oxygen oversaturation” was simulated only in spring and early summer, when algal bloom events were also most frequently observed [32,47]. In addition, the results for NH₃-N and NO₃-N also showed a similar consumption pattern to that seen with the growth of algae (Figure 7a–d).

3.2. Evaluating the Risks to Water Quality due to Climate Change

Although the uncertainty analysis for W2 model is not provided in this work, the W2 model structure and its parameter settings have been tested to be sensitive to climate drivers, and is a suitable tool for the prediction of climate change impacts on reservoir/lake hydrodynamic and water quality parameters [14,24]. In actuality, there are many sources of uncertainty in evaluating climate change impacts on freshwater resources, including parametric uncertainty, model structure uncertainty and the selected climate data [52]. Generally, a consensus has been reached among researchers that the climate change data and its associated decision procedures, such as the choice of global climate models (GCMs), emissions scenario, and downscaling methodology, are commonly the largest source of uncertainty when the projected climate data and hydrodynamic/water quality model are integrated for the evaluation of climate change impacts [53–55]. Furthermore, uncertainties due to the model parameters and structure are concluded to be relatively less important if variation for the climate outputs from different GCMs is considered [53,55]. Therefore, the possible variation for the future prediction of water quality parameters are estimated in this study by evaluating the uncertainty induced by the selection of climate outputs from 24 AOGCM outputs (as described in Section 2.3). As a result, the exceedance probability estimated from the climate ensemble, and the 95% confidence interval for the average value computed by all selected climate outputs (Table 1), are both reported in this section. The uncertainty ranges can represent the possible variations of hydrodynamic and water quality state variables for future predictions.

3.2.1. Water Temperature

Temperature is regarded as an important factor that can induce algal blooms [13,56]. There will thus be a higher risk of algal blooms if the projected surface water exceeds a temperature threshold. In this study, temperature thresholds of 18, 25, and 32 °C were used to assess the risk to water quality. The risk exceedance probabilities for the water surface temperature are listed in Table 4. The results indicate that the projected changes in climate will significantly raise the water temperature (relative to the 2004–2012 period), and increase the risk of developing associated water quality problems in HSR. The probability that surface water temperature would exceed 32 °C is projected to increase by 2.6% and 10.6% for the short- and long-term future under the A2 scenario (a better-than-worst case),

respectively. Compared with the water temperature in the 2004–2012 period, the increased exceedance probabilities in extremes (low and high) are greater than that seen in a medium temperature range (25 °C) (Table 4). For example, the probabilities that surface water temperature would exceed 32, 25, and 18 °C are projected to increase by 9.2%, 7.7%, and 11.7% for the long-term future under the A1B scenario (a balanced case), respectively.

Table 4. Risk exceedance probability for the surface water temperature and DO.

Parameter	Value	Ranking	Risk Exceedance Probability (%)				
			2004–2012	2020–2039		2080–2099	
				A1B	A2	A1B	A2
Temperature (°C)	18	Low	79.2	82.7 (81.1–84.2)	81.8 (79.9–83.7)	90.9 (89.6–92.1)	90.8 (87.3–94.4)
	25	Medium	43.2	45.2 (43.9–46.6)	44.8 (43.4–46.2)	50.9 (49.4–52.5)	51.5 (49.0–54.0)
	32	High	9.4	11.8 (9.9–13.6)	12.0 (11.1–12.9)	18.6 (17.4–19.7)	20.0 (16.7–23.2)
DO (mg/L)	6	Low	98.7	98.7 (98.6–98.8)	98.7 (98.6–98.7)	98.8 (98.7–98.8)	98.8 (98.6–98.8)
	8.5	Medium	45.9	44.6 (43.5–45.6)	45.2 (44.1–46.3)	39.9 (38.1–41.7)	39.8 (37.8–41.8)
	11	High	6.3	6.3 (6.2–6.4)	6.4 (6.2–6.5)	5.9 (5.7–6.2)	5.9 (5.5–6.3)

Note: The values in brackets (left to right) are confidence interval lower and upper bounds, respectively.

In addition, we examine the projected differences between surface- and bottom-layer temperatures to assess the impacts of climate change on seasonal thermal stratification. As shown in Table 5, the differences between water temperature at the surface and bottom layer are estimated to increase by 0.01 and 0.75 °C in summer for the short- and long-term future, respectively. Consequently, the thermal stratification in summertime will be both longer and stronger, which can enhance anoxia in deep layers and may increase the release of phosphorus from sediment [2].

Table 5. The projected seasonal temperature and DO differences between surface and bottom layers.

Parameter	Period	Spring	Summer	Fall	Winter
Temperature (°C)	2004–2012	3.13	10.84	6.59	0.62
	2020–2039	3.16	10.85	6.62	0.62
	2080–2099	3.53	11.59	7.61	0.94
DO (mg/L)	2004–2012	2.67	7.31	7.31	1.47
	2020–2039	2.86	7.44	7.44	1.75
	2080–2099	3.38	7.7	7.7	2.6

3.2.2. DO

DO is a temperature-associated parameter. Increased temperature will reduce DO saturation levels and increase the risk of oxygen depletion [57]. The projected risks for DO at the surface layer exceeding thresholds of 6, 8.5 and 11 mg/L are listed in Table 4. Compared to the significant change in water temperature, the change in surface DO is relatively minor. However, the level of surface DO is expected to decrease significantly in the long-term future (2080–2099), due to a stronger increase in surface water temperature (likely ranging from 1.6 to 1.8 °C). For example, under the A1B scenario, the risk exceedance probability for surface DO at a threshold of 8.5 mg/L is projected to decrease by

1.3% (95% confidence interval (CI), 0.3 to 2.4) and 6.0% (95% CI, 4.2 to 7.8) for the short- and long-term future, respectively. Although the increased temperature decreases the DO content of water, the results indicate that the surface DO will still commonly be kept at a saturation level under the projected changes in climate.

The projected divergence between surface- and bottom-layer DO for each season is shown in Table 5. The difference between surface- and bottom-layer DO is expected to be stronger during the stratification season under the projected changes in climate, which will increase by between 0.1 and 0.3 mg/L for the near future, and 0.3 to 0.9 mg/L for the long-term future. As a result, the projected increase in thermal stratification will lead to a stronger DO stratification in HSR.

3.2.3. Nutrients

Table 6 shows the projected risks of ortho-P and TP in the surface and bottom layers exceeding the threshold values. The results show that climate change has an obvious impact on risk to ortho-P and TP, the limiting nutrient of algal growth in HSR. Relative to the 2004–2012 time period, the probability that ortho-P in the surface layer would exceed the medium threshold is projected to increase by 6.8% and 13.8% for the short- and long-term future under the A1B scenario, respectively, representing 10.0% and 16.9% increases with regard to TP under the same conditions. The exceedance probabilities for bottom layer ortho-P and TP at the same threshold value are much greater than that within surface layer. For example, the projected changes in the level of ortho-P in the bottom layer are approximately five times greater than those in surface layer under the A1B scenario, because of the increased oxygen stratification and depletion in HSR.

The simulation results of water quality state variables during the base-period (2004–2012) indicate that ortho-P and TP at the water surface decreased while the temperature and DO were stratified in HSR during summer (Figure 6a,b). The peak ortho-P and TP concentrations in surface layer have often been simulated during the turnover periods (winter and spring), due to the upwelling of nutrient-rich hypolimnion water. Therefore, this suggests that the key source of phosphorus in HSR is in fact its release from sediment.

Table 7 shows the projected risks of NH₃-N and NO₃-N in surface and bottom layers exceeding the threshold values due to changes in climate. The results indicate that NH₃-N in the bottom layer is expected to increase, but the projected level of NH₃-N in the surface layer and NO₃-N in the entire water column both show a decreasing trend in the future. The lower estimated nitrate concentrations might be attributed to the increased rates of algal growth and bacteria denitrification, as well as the extended growing period of aquatic plants under the warmer climate [58]. In HSR, the increased consumption of phosphorus can be compensated or even exceeded by the projected increase in phosphorus flux from sediment. However, according to the decreasing trend of nitrogen, it is evident that the supply of nitrogen from different sources is less than the increased consumption due to the warmer climate.

Table 6. Risk exceedance probability for the levels of phosphorus in surface and bottom layers, and Chl-*a* at surface.

Nutrient	Layer	Threshold (mg/L)	Ranking	Exceedance Probability (%)				
				2004–2012	2020–2039		2080–2099	
					A1B	A2	A1B	A2
PO ₄ ³⁻	Surface	0.015	Low	24.8	26.4 (26.0–26.8)	26.4 (26.1–26.8)	25.5 (25.1–25.9)	25.1 (25.1–26.3)
		0.020	Medium	13.1	20.4 (19.0–21.7)	20.7 (20.6–20.8)	21.0 (20.5–21.4)	20.8 (20.0–21.4)
		0.025	High	2.6	9.4 (6.7–12.0)	7.9 (6.1–9.7)	16.4 (15.0–17.9)	15.9 (13.8–17.1)
	Bottom	0.015	Low	99.6	99.8 (99.7–99.8)	99.8 (99.76–99.84)	99.9 (99.8–99.9)	99.9 (99.9–99.9)
		0.020	Medium	92.0	96.2 (94.1–98.3)	95.8 (94.4–97.3)	98.0 (97.0–99.1)	98.4 (98.2–98.5)
		0.025	High	49.8	71.8 (58.5–85.1)	67.4 (58.3–76.5)	89.9 (80.9–98.9)	92.1 (89.8–94.3)
TP	Surface	0.012	Low	81.6	85.7 (83.3–88.0)	85.4 (82.6–88.3)	93.8 (92.5–95.1)	93.0 (91.3–94.7)
		0.024	Medium	38.6	48.6 (45.7–51.5)	47.5 (44.7–50.2)	55.5 (54.3–56.7)	56.0 (53.7–58.4)
		0.035	High	4.7	9.1 (6.2–11.9)	6.9 (5.6–8.2)	22.3 (22.2–22.5)	21.5 (14.8–25.7)
	Bottom	0.012	Low	100	100 (99.2–100)	100 (98.5–100)	100 (99.4–100)	100 (99.1–100)
		0.024	Medium	96.2	98.7 (97.4–100)	98.3 (97.1–99.4)	100 (99.3–100)	100 (98.6–100)
		0.035	High	19.4	35.2 (23.3–47.0)	29.6 (24.2–35.1)	63.2 (42.4–84.0)	65.4 (53.4–77.3)
Chl- <i>a</i>	Surface	0.003	Oligotrophic	66.3	71.7 (70.3–73.1)	71.3 (69.2–73.5)	73.8 (72.8–74.7)	75.3 (73.8–76.7)
		0.007	Mesotrophic	14.2	20.3 (17.9–22.6)	18.9 (16.7–21.1)	28.5 (27.9–29.1)	28.4 (26.3–30.5)
		0.010	Eutrophic	2.7	5.4 (4.4–6.4)	4.5 (3.6–5.4)	9.8 (9.5–10.1)	9.0 (7.4–10.6)

Note: The values in brackets (left to right) are confidence interval lower and upper bounds, respectively.

Table 7. Risk exceedance probability for the levels of nitrogen in surface and bottom layers.

Nutrient	Layer	Threshold (mg/L)	Ranking	Exceedance Probability (%)				
				2004–2012	2020–2039		2080–2099	
					A1B	A2	A1B	A2
NH ₃ -N	Surface	0.01	Low	92.2	82.5 (81.4–83.5)	82.5 (81.5–83.5)	84.9 (83.8–86.0)	85.7 (84.7–86.7)
		0.03	Medium	29.6	11.8 (9.4–14.3)	10.6 (9.0–12.2)	17.2 (14.2–20.3)	17.6 (15.5–18.9)
		0.04	High	9.3	1.3 (1.1–1.5)	1.2 (1.0–1.4)	1.8 (1.3–2.4)	1.7 (1.5–2.0)
	Bottom	0.01	Low	31.9	37.1 (33.8–40.4)	36.5 (34.0–39.1)	45.1 (41.3–48.9)	47.3 (45.8–48.8)
		0.03	Medium	6.7	9.1 (7.7–10.4)	8.8 (7.5–10.1)	14.6 (11.5–17.7)	14.8 (12.5–17.1)
		0.04	High	5.1	6.7 (5.7–7.6)	6.3 (5.3–7.4)	10.2 (8.4–11.9)	10.7 (9.5–11.9)
NO ₃ -N	Surface	0.2	Low	94.8	91.4 (89.9–93.0)	91.9 (89.9–93.8)	84.9 (83.3–86.6)	82.8 (79.7–86.0)
		0.5	Medium	41.1	31.3 (29.4–33.2)	31.2 (28.5–34.0)	24.7 (23.1–26.3)	23.9 (21.8–26.0)
		0.7	High	8.9	6.7 (6.3–7.2)	6.8 (6.2–7.4)	5.3 (5.0–5.7)	5.2 (5.1–5.3)
	Bottom	0.2	Low	98.8	97.4 (96.3–98.5)	97.7 (96.7–98.7)	91.2 (87.9–94.5)	90.6 (87.9–93.3)
		0.5	Medium	61.7	56.7 (53.7–59.7)	56.9 (53.5–60.3)	45.3 (40.7–49.8)	44.0 (39.2–48.9)
		0.7	High	17.3	12.7 (11.5–13.9)	13.3 (11.5–15.1)	10.3 (9.7–11.0)	10.2 (9.5–10.9)

Note: The values in brackets (left to right) are confidence interval lower and upper bounds, respectively.

The overgrowth of algae in natural freshwater ecosystems is often determined by the available internal phosphorus flux [59]. In HSR, the predicted thermal stratification may keep phosphorus at the bottom and prevent the occurrence of algal blooms in summer, as shown on the observed/simulated phosphorus trends during the base period (Figure 6c–f). The upwelling of nutrient-rich water can support the overgrowth of algae during periods of non-stratification, although this is limited by the unfavorable growing temperature [60] in HSR. Therefore, the frequency of algal bloom events is predicted to increase during the springtime, when the temperature is getting warmer and thermal stratification has not yet occurred. In addition, the enhanced anoxia in deep layers caused by increased thermal stratification will aggravate the release of phosphorus from sediment. The probability of TP in the surface layer exceeding 0.024 mg/L, the threshold of eutrophication in Carlson's Trophic State Index (CTSI) [48], is more than 47.5% for both the near- and long-term future (Table 6).

3.2.4. Chlorophyll-*a*

The probability that Chl-*a* will exceed 7.2 µg/L, the threshold of eutrophication in CTSI, is only 14.2% during the base-period (2004–2012) in HSR (Table 6), indicating that HSR is generally in a mesotrophic state. However, changes in climate will significantly increase the concentrations of Chl-*a*. As shown on Table 6, the risks of Chl-*a* exceeding 7.2 µg/L in the near- and long-term future are estimated to increase by 6.1% (95% CI, 3.7 to 8.4) and 14.3% (95% CI, 13.7 to 14.9) under the A1B scenario, respectively. The occurrences of extreme temperature (>32 °C) (Table 4) and high phosphorus concentrations in the surface layer (>0.025 mg/L) (Table 6) are both predicted to increase, resulting in a higher risk of eutrophication and algal events in HSR. For example, the risk of Chl-*a* exceeding 10.0 µg/L in the long-term future will increase by 7.1% (95% CI, 6.8 to 7.4) under the A1B scenario.

Although Chl-*a* and TP are both projected to increase, there is still a difference between them with regard to the risk of exceeding the eutrophication threshold of CTSI. Compared to the use of Chl-*a* as an eutrophication indicator, the surface water is easier to be determined as being in a eutrophic state using TP (Table 6). For example, the risk of TP exceeding 0.035 mg/L is 4.7%, 9.1%, and 22.3% for the base, near- and long-term periods under the A1B scenario, respectively, which are approximately two times greater than the risk of Chl-*a* exceeding 0.010 mg/L. It is concluded that the presence of phosphorus in HSR exceeds the level required by the algae to achieve a eutrophic state [6]. There are other factors limiting the growth of algae in certain circumstances, such as the water temperature or sunlight. In HSR, the levels of ortho-P or TP are supposed to limit the growth of algae when the reservoir is stratified. However, during periods of non-stratification (*i.e.*, when the water is well-mixed), the surface water temperature is the limiting factor for the overgrowth of algae [61].

4. Conclusions

This study assessed the impacts of climate change on the risks to water quality of a small deep reservoir in a humid-subtropical climatic region under the greenhouse gas emission scenarios of A1B and A2. The projected changes in water quality for the near (2020–2039) and long-term (2080–2099) future are estimated by CE-QUAL-W2 model with downscaled future climate data. The results indicate that rising temperatures will significantly lower the water quality in HSR through greater

thermal stability and DO stratification, resulting in reduced DO concentrations in deeper layers of the reservoir and increased release of phosphorus from sediments. This flux in phosphorus in the hypolimnion may not support algal growth in the epilimnion during summer. However, nutrients are projected to increase throughout the reservoir, since it is well-mixed in late fall/winter. However, even more critical for reservoir managers is the projected earlier arrival of spring. If the presence of nutrients is high, the prolonged growing season will increase the expected frequency of algal blooms.

In HSR it would be advantageous to inhibit the upwelling of nutrients available to algae during the growing season, therefore conventional aeration approaches which involve the breaking up of thermal stratification may actually have negative impacts on water quality. Two adaptation strategies are thus suggested. First, management strategies that apply hypolimnetic aeration are recommended so as to increase bottom-layer DO without destratification [62]. The second suggested strategy involves lowering the height of the inlet to the depth of the hypolimnion layer formed during the stratification period. This will prevent the overgrowth of algae from the direct supply of nutrient-rich recharge water [7,33], and so can be used to address to the issue of anoxia in deeper layers.

It should be noted, however, that this study did not consider the projected changes in the quantity and quality of the recharged water (pumped from the Keelung River), and the modeling results do not reflect the impacts of climate change on the Keelung River catchment. Future work that links the outputs of catchment hydrology and the water quality model with W2 is thus required to comprehensively assess the impacts of climate change on the risks to water quality in HSR.

Acknowledgments

The authors are grateful to the Taiwan Climate Change Projection and Information Platform, which provided climate change projection data for this research. This research was supported in part by Water Research Foundation (Project 4468), Water Research Australia (1050-11), Taiwan Water Corporation, and the Headquarters of University Advancement at the National Cheng Kung University, which is sponsored by the Ministry of Education, Taiwan, ROC.

Author Contributions

Chih-Hua Chang and Long-Yan Cai conducted W2 modeling approach, analyzed data and wrote the paper. Tsair-Fuh Lin participated in proofreading the article and supervised the project. Chia-Ling Chung and Leon van der Linden performed the W2 simulation and climate data downscaling, and Michael Burch supervised the project.

Conflicts of Interest

The authors declare no conflict of interest.

References

1. Intergovernmental Panel on Climate Change (IPCC). *Climate Change 2007: The Physical Science Basis*; Cambridge University Press: Cambridge, UK; New York, NY, USA, 2007; p. 996.

2. Jones, J.; Brett, M.T. Lake nutrients, eutrophication, and climate change. In *Global Environmental Change*; Springer: New York, NY, USA, 2014; pp. 273–279.
3. Intergovernmental Panel on Climate Change (IPCC). *Managing the Risks of Extreme Events and Disasters to Advance Climate Change Adaptation*; Cambridge University Press: Cambridge, UK; New York, NY, USA, 2012; p. 582.
4. Huntington, T.G. Evidence for intensification of the global water cycle: Review and synthesis. *J. Hydrol.* **2006**, *319*, 83–95.
5. Stockholm International Water Institute (SIWI). *The Role of Large Scale Artificial Water Storage in the Water-Food-Energy Development Nexus*; SIWI: Stockholm, Sweden, 2009; p. 38.
6. Deus, R.; Brito, D.; Mateus, M.; Kenov, I.; Fornaro, A.; Neves, R.; Alves, C. Impact evaluation of a pisciculture in the Tucuruí Reservoir (Pará, Brazil) using a two-dimensional water quality model. *J. Hydrol.* **2013**, *487*, 1–12.
7. Chung, S.; Oh, J. Calibration of CE-QUAL-W2 for a monomictic reservoir in a monsoon climate area. *Water Sci. Technol.* **2006**, *54*, 29–37.
8. Park, Y.; Cho, K.H.; Kang, J.-H.; Lee, S.W.; Kim, J.H. Developing a flow control strategy to reduce nutrient load in a reclaimed multi-reservoir system using a 2D hydrodynamic and water quality model. *Sci. Total Environ.* **2014**, *466*, 871–880.
9. Brooks, B.; Valenti, T.; Cook-Lindsay, B.; Forbes, M.; Doyle, R.; Scott, J.; Stanley, J. Influence of climate change on reservoir water quality assessment and management. In *Climate*; Springer: New York, NY, USA, 2011; pp. 491–522.
10. Molina-Navarro, E.; Trolle, D.; Martínez-Pérez, S.; Sastre-Merlín, A.; Jeppesen, E. Hydrological and water quality impact assessment of a mediterranean limno-reservoir under climate change and land use management scenarios. *J. Hydrol.* **2014**, *509*, 354–366.
11. Varis, O.; Somlyódy, L. Potential impacts of climate change on lake and reservoir water quality. In *Water Resources Management in the Face of Climatic/Hydrologic Uncertainties*; Kaczmarek, Z., Strzepek, K.M., Somlyódy, L., Priazhinskaya, V., Eds.; Kluwer Academic Publishers: Amsterdam, The Netherlands, 1996.
12. Sahoo, G.; Schladow, S.; Reuter, J.; Coats, R. Effects of climate change on thermal properties of lakes and reservoirs, and possible implications. *Stoch. Env. Res. Risk A* **2011**, *25*, 445–456.
13. Duan, H.; Ma, R.; Xu, X.; Kong, F.; Zhang, S.; Kong, W.; Hao, J.; Shang, L. Two-decade reconstruction of algal blooms in China's Lake Taihu. *Environ. Sci. Technol.* **2009**, *43*, 3522–3528.
14. Thorne, O.; Fenner, R. The impact of climate change on reservoir water quality and water treatment plant operations: A UK case study. *Water Environ. J.* **2011**, *25*, 74–87.
15. Zhu, M.; Zhu, G.; Zhao, L.; Yao, X.; Zhang, Y.; Gao, G.; Qin, B. Influence of algal bloom degradation on nutrient release at the sediment-water interface in Lake Taihu, China. *Environ. Sci. Pollut. R.* **2013**, *20*, 1803–1811.
16. Arheimer, B.; Andréasson, J.; Fogelberg, S.; Johnsson, H.; Pers, C.B.; Persson, K. Climate change impact on water quality: Model results from southern Sweden. *AMBIO* **2005**, *34*, 559–566.
17. Trolle, D.; Hamilton, D.P.; Pilditch, C.A.; Duggan, I.C.; Jeppesen, E. Predicting the effects of climate change on trophic status of three morphologically varying lakes: Implications for lake restoration and management. *Environ. Modell. Softw.* **2011**, *26*, 354–370.

18. Carvalho, L.; Miller, C.; Spears, B.; Gunn, I.; Bennion, H.; Kirika, A.; May, L. Water quality of Loch Leven: Responses to enrichment, restoration and climate change. *Hydrobiologia* **2012**, *681*, 35–47.
19. Schindler, D.W.; Bayley, S.E.; Parker, B.R.; Beaty, K.G.; Cruikshank, D.R.; Fee, E.J.; Schindler, E.U.; Stainton, M.P. The effects of climatic warming on the properties of boreal lakes and streams at the experimental lakes area, northwestern Ontario. *Limnol. Oceanogr.* **1996**, *41*, 1004–1017.
20. Kim, B.; Park, J.-H.; Hwang, G.; Jun, M.-S.; Choi, K. Eutrophication of reservoirs in South Korea. *Limnology* **2001**, *2*, 223–229.
21. Jones, P.D.; New, M.; Parker, D.E.; Martin, S.; Rigor, I.G. Surface air temperature and its changes over the past 150 years. *Rev. Geophys.* **1999**, *37*, 173–199.
22. Shiu, C.-J.; Liu, S.C.; Chen, J.-P. Diurnally asymmetric trends of temperature, humidity, and precipitation in Taiwan. *J. Clim.* **2009**, *22*, 5635–5649.
23. Hsu, H.-H.; Chen, C.-T. Observed and projected climate change in Taiwan. *Meteorol. Atmos. Phys.* **2002**, *79*, 87–104.
24. Tseng, H.-W.; Yang, T.-C.; Kuo, C.-M.; Yu, P.-S. Application of multi-site weather generators for investigating wet and dry spell lengths under climate change: A case study in southern Taiwan. *Water Resour. Manag.* **2012**, *26*, 4311–4326.
25. Afshar, A.; Kazemi, H.; Saadatpour, M. Particle swarm optimization for automatic calibration of large scale water quality model (CE-QUAL-W2): Application to Karkheh Reservoir, Iran. *Water Resour. Manag.* **2011**, *25*, 2613–2632.
26. Cole, T.M.; Tillman, D.H. *Water Quality Modeling of Lake Monroe Using CE-QUAL-W2*; U.S. Army Engineer Waterways Experiment Station: Louisville, KY, USA, 1999; p. 94.
27. Deus, R.; Brito, D.; Kenov, I.A.; Lima, M.; Costa, V.; Medeiros, A.; Neves, R.; Alves, C. Three-dimensional model for analysis of spatial and temporal patterns of phytoplankton in Tucuruí Reservoir, Pará, Brazil. *Ecol. Model.* **2013**, *253*, 28–43.
28. Giorgi, F.; Mearns, L.O. Calculation of average, uncertainty range, and reliability of regional climate changes from AOGCM simulations via the reliability ensemble averaging (REA) method. *J. Clim.* **2002**, *15*, 1141–1158.
29. Harding, B.; Wood, A.; Prairie, J. The implications of climate change scenario selection for future streamflow projection in the upper Colorado River Basin. *Hydrol. Earth Syst. Sci.* **2012**, *9*, 847–894.
30. Chiew, F.; Teng, J.; Vaze, J.; Post, D.; Perraud, J.; Kirono, D.; Viney, N. Estimating climate change impact on runoff across southeast Australia: Method, results, and implications of the modeling method. *Water Resour. Res.* **2009**, *45*, doi:10.1029/2008WR007338.
31. Zhang, Y.; Wu, Z.; Liu, M.; He, J.; Shi, K.; Zhou, Y.; Wang, M.; Liu, X. Dissolved oxygen stratification and response to thermal structure and long-term climate change in a large and deep subtropical reservoir (Lake Qiandaohu, China). *Water Res.* **2015**, *75*, 249–258.
32. Wu, S.C.; Wu, J.T.; Chang, M.I. *Correlation of Algae Eutrophication Indicators and Water Quality in Hsinshan Reservoir (2010)*; Taiwan Water Corporation: Taichung, Taiwan, 2010. (In Chinese).

33. Cole, T.M.; Scott, A.W. *CE-QUAL-W2: A Two-Dimensional, Laterally Averaged, Hydrodynamic and Water Quality Model*; Version 3.71 User manual; U.S. Army Engineer Waterways Experiment Station: Louisville, KY, USA, 2013; p. 783.
34. Mateus, M.; Almeida, C.; Brito, D.; Neves, R. From eutrophic to mesotrophic: Modelling watershed management scenarios to change the trophic status of a reservoir. *Int. J. Environ. Res. Public Health* **2014**, *11*, 3015–3031.
35. Debele, B.; Srinivasan, R.; Parlange, J.-Y. Coupling upland watershed and downstream waterbody hydrodynamic and water quality models (SWAT and CE-QUAL-W2) for better water resources management in complex river basins. *Environ. Model. Assess.* **2008**, *13*, 135–153.
36. Huang, Y.T.; Liu, L. A Hybrid perturbation and Morris approach for identifying sensitive parameters in surface water quality models. *J. Environ. Inform.* **2008**, *12*, 150–159.
37. Chang, C.H.; Wen, C.G.; Huang, C.H.; Chang, S.P.; Lee, C.S. Nonpoint source pollution loading from an undistributed tropic forest area. *Environ. Monit. Assess.* **2008**, *146*, 113–126.
38. Lee, C.S.; Chang, C.H.; Wen, C.G.; Chang, S.P. Comprehensive nonpoint source pollution models for a free-range chicken farm in a rural watershed in Taiwan. *Agric. Ecosyst. Environ.* **2010**, *139*, 23–32.
39. Wood, A.W.; Maurer, E.P.; Kumar, A.; Lettenmaier, D.P. Long-range experimental hydrologic forecasting for the eastern United States. *J. Geophys. Res. Atmos.* **2002**, *107*, doi:10.1029/2001JD000659.
40. Chiew, F.; Kirono, D.; Kent, D.; Frost, A.; Charles, S.; Timbal, B.; Nguyen, K.; Fu, G. Comparison of runoff modelled using rainfall from different downscaling methods for historical and future climates. *J. Hydrol.* **2010**, *387*, 10–23.
41. Wetterhall, F.; Pappenberger, F.; He, Y.; Freer, J.; Cloke, H.L. Conditioning model output statistics of regional climate model precipitation on circulation patterns. *Nonlinear Proc. Geoph.* **2012**, *19*, 623–633.
42. Post, D.; Chiew, F.; Yang, A.; Viney, N.; Vaze, J.; Teng, J. The hydrologic impact of daily versus seasonal scaling of rainfall in climate change studies. In *Interfacing Modelling and Simulation with Mathematical and Computational Sciences*, Proceedings of the 18th World IMACS/MODSIM Congress, Cairns, Australia, 13–17 July 2009.
43. Lin, L.-Y. A user-based climate change service project: Taiwan climate change projection and information platform project (TCCIP). In Proceedings of the 20th IHDP Scientific Committee Meeting, Taipei, Taiwan, 16–18 May 2013.
44. Intergovernmental Panel on Climate Change (IPCC). *Emissions Scenarios*; Cambridge University Press: Cambridge, UK; New York, NY, USA, 2000.
45. Environmental Protection Administration (EPA, Taiwan). The Environmental Water Quality Information System. Available online: <http://wq.epa.gov.tw/WQEPA/Code/?Languages=en> (accessed on 6 April 2015).
46. Taiwan Environmental Analysis Laboratory. The Standard Methods for the Examination of Water and Wastewater. Available online: <http://www.niea.gov.tw/> (accessed on 6 April 2015).
47. Wu, S.C.; Wu, J.T.; Chang, M.I. *Correlation of Algae Eutrophication Indicators and Water Quality in Hsinshan Reservoir (2011)*; Taiwan Water Corporation: Taichung, Taiwan, 2011. (In Chinese).

48. Calson, R.E. A trophic state index for lakes. *Limnol. Oceanogr.* **1977**, *22*, 361–369.
49. Badran, M.I. Dissolved oxygen, chlorophyll a and nutrients: Seasonal cycles in waters of the Gulf of Aquaba, Red Sea. *Aquat. Ecosyst. Health* **2001**, *4*, 139–150.
50. Martin, S.C.; Effler, S.W.; DePinto, J.V.; Trama, F.B.; Rodgers, P.W.; Dobi, J.S.; Wodka, M.C. Dissolved oxygen model for a dynamic reservoir. *J. Environ. Eng. ASCE* **1985**, *111*, 647–664.
51. Carpenter, S.R. Phosphorus control is critical to mitigating eutrophication. *Proc. Natl. Acad. Sci. USA* **2008**, *105*, 11039–11040.
52. Lindenschmidt, K.E.; Fleischbein, K.; Baborowski, M. Structural uncertainty in a river water quality modelling system. *Ecolog. Model.* **2007**, *204*, 289–300.
53. Kay, A.L.; Davies, H.N.; Bell, V.A.; Jones, R.G. Comparison of uncertainty sources for climate change impacts: flood frequency in England. *Clim. Change* **2009**, *92*, 41–63.
54. Horton, P.; Schaepli, B.; Mezghani, A.; Hingray, B.; Musy, A. Assessment of climate-change impacts on alpine discharge regimes with climate model uncertainty. *Hydrol. Process* **2006**, *20*, 2091–2109.
55. Wilby, R. L.; Harris, I. A framework for assessing uncertainties in climate change impacts: Low-flow scenarios for the River Thames, UK. *Water Resour. Res.* **2006**, *42*, doi:10.1029/2005WR004065.
56. Kanoshina, I.; Lips, U.; Leppänen, J.-M. The influence of weather conditions (temperature and wind) on cyanobacterial bloom development in the Gulf of Finland (Baltic Sea). *Harmful Algae* **2003**, *2*, 29–41.
57. Foley, B.; Jones, I.D.; Maberly, S.C.; Rippey, B. Long-term changes in oxygen depletion in a small temperate lake: Effects of climate change and eutrophication. *Freshwater Biol.* **2012**, *57*, 278–289.
58. Bates, B.C.; Kundzewicz, Z.W.; Wu, S.; Palutikof, J.P. Climate change and water. In *Technical Paper of the Intergovernmental Panel on Climate Change*; Intergovernmental Panel on Climate Change (IPCC): Geneva, Switzerland, 2008; p. 210.
59. Nikolai, S.J.; Dzialowski, A.R. Effects of internal phosphorus loading on nutrient limitation in a eutrophic reservoir. *Limnologica* **2014**, *49*, 33–41.
60. Robarts, R.D.; Zohary, T. Temperature effects on photosynthetic capacity, respiration, and growth rates of bloom-forming cyanobacteria. *N. Z. J. Mar. Freshwater Res.* **1987**, *21*, 391–399.
61. Huang, J.C.; Gao, J.F.; Mooij, W.M.; Hörmann, G.; Fohrer, N. A comparison of three Approaches to predict phytoplankton biomass in Gonghu Bay of Lake Taihu. *J. Environ. Inform.* **2014**, *24*, 39–51.
62. Singleton, V.L.; Little, J.C. Designing hypolimnetic aeration and oxygenation systems—A review. *Environ. Sci. Technol.* **2006**, *40*, 7512–7520.